Klein M, Chakraborty N.

***A-priori* analysis of an alternative wrinkling factor definition for flame surface density based Large Eddy Simulation modelling of turbulent premixed combustion.**

***Combustion Science and Technology* 2018**

DOI: https://doi.org/10.1080/00102202.2018.1452394

A-priori analysis of an alternative wrinkling factor definition for Flame Surface Density based Large Eddy Simulation modelling of turbulent premixed combustion

Markus Klein*[a] and Nilanjan Chakraborty**

*Department of Aerospace Engineering, Universität der Bundeswehr München, Neubiberg, 85577, Germany

**School of Mechanical & Systems Engineering, Newcastle University, Newcastle-Upon-Tyne, NE1 7RU, UK

*[a] Corresponding author

Tel.: +49 89/6004-2122

Fax: +49 89/6004-2135

E-mail: markus.klein@unibw.de

Keywords: Flame Surface Density, Wrinkling Factor, Large Eddy Simulation, Premixed combustion, Direct Numerical Simulation

ABSTRACT

This paper discusses an alternative definition of the wrinkling factor and the resolved component of flame surface density (FSD) in the context of Large Eddy Simulations (LES) modelling of turbulent premixed combustion. The performances of conventional and an alternative definition of wrinkling factor are compared by employing a-priori analysis using explicitly filtered direct numerical simulation (DNS) data of statistically planar turbulent premixed, flames. It is demonstrated that the alternative definition of wrinkling factor can be used as well as the conventional definition to model the sub-grid scale flame wrinkling. The conventional definition of the wrinkling factor and resolved FSD might be more satisfactory from a theoretical point of view but the alternative definition has the advantage that the resolved FSD is no longer an unclosed expression and artificial flame thickening can be avoided without referring to an implicit counter-gradient transport closure.

Keywords: Flame Surface Density, Wrinkling factor, Large Eddy Simulations, A-priori analysis, Turbulent premixed flame

1. INTRODUCTION

The complexity of the system of partial differential equations describing turbulent reactive flows gives rise to unclosed terms in the context of Large Eddy Simulation (LES). In LES, the filtering (denoted by $\overline{\cdot}$) and Favre filtering (denoted by $\widetilde{\cdot}$) operation of a quantity $\boldsymbol{Q}$ with a Gaussian filter kernel $\boldsymbol{G}(\boldsymbol{r})$ are given as:

$$\overline{Q(\boldsymbol{x})} = \int Q(\boldsymbol{x}-\boldsymbol{r})G(\boldsymbol{r})\boldsymbol{dr}, \;\; G(\boldsymbol{r}) = (6/\pi\Delta^2)^{3/2}\exp(-6\,\boldsymbol{r}\cdot\boldsymbol{r}\,/\Delta^2), \qquad \tilde{Q} = \overline{\rho Q}/\bar{\rho} \qquad (1)$$

In Eq. 1, Δ denotes the filter width. The mass fractions of the reactive species in a premixed flame can be utilised to define a reaction progress variable c assuming the values $c = 0$ on the reactant side and $c = 1$ in the fully burned products (Peters, 2000). In this framework, the transport equation for the filtered reaction progress can be written as:

$$\partial(\bar{\rho}\tilde{c})/\partial t + \nabla\cdot(\bar{\rho}\tilde{\boldsymbol{u}}\tilde{c}) = -\nabla\cdot(\overline{\rho\boldsymbol{u}c} - \bar{\rho}\tilde{\boldsymbol{u}}\tilde{c}) + \overline{\nabla\cdot(\rho D\nabla c) + \dot{\omega}_c}\,. \qquad (2)$$

Here $\rho, \boldsymbol{u}, D$ and $\dot{\omega}_c$ denote density, velocity, progress variable diffusivity and reaction rate respectively. Both terms on the right hand side of eq. 2 are unclosed. The sub-grid scalar flux (SGSF) of reaction progress variable is given by:

$$\overline{\rho\boldsymbol{u}c} - \bar{\rho}\tilde{\boldsymbol{u}}\tilde{c} \qquad (3)$$

The modelling of sub-grid scalar flux has been discussed recently by the authors (Gao *et al.*, 2015; Klein *et al.*, 2016a). The closure of eq. 2 also needs the modelling of the filtered flame front displacement (FFFD):

$$\overline{\nabla\cdot(\rho D\nabla c) + \dot{\omega}_c} \qquad (4)$$

A-priori and *a-posteriori* assessment of the FFFD terms have been addressed in Chakraborty and Klein (2008) and Ma *et al.* (2013). Interested readers are directed to Gao *et al.* (2015), Klein *et al.* (2016b), Chakraborty and Klein (2008) and Ma *et al.* (2013) and references therein for a detailed review of the existing literature. It is worth noting that models for both the FFFD and SGSF terms interact with each other and the best overall model is not necessarily given by the combination of the best individual model expressions, as discussed in Klein *et al.* (2016b).

A variety of concepts exist to deal with the closure of turbulent premixed combustion such as the *G*-equation (Pitsch *et al.*, 2002) or the artificially thickened flame concept (Colin *et al.*, 2000). In this work we focus on the flame surface density (FSD) approach, where the FFFD term is expressed as:

$$\overline{\nabla \cdot (\rho D \nabla c) + \dot{\omega}_c} = \overline{(\rho S_d)}_S \, \Sigma_{\text{gen}} = \overline{(\rho S_d)}_S \, \Xi \, |\nabla \bar{c}| \quad ; \quad \Xi = \overline{|\nabla c|}/|\nabla \bar{c}| \, ; \quad \Sigma_{\text{gen}} = \overline{|\nabla c|} \qquad (5)$$

Here S_d is the displacement speed of a given *c* isosurface, Ξ is the wrinkling factor and Σ_{gen} is the generalised flame surface density FSD (Boger *et al.*, 1998). The surface-weighted filtering operation $\overline{(\cdot)}_S$ for a general quantity Q is given by (Boger *et al.*, 1998):

$$\overline{(Q)}_S = \overline{Q|\nabla c|}/\,\overline{|\nabla c|} \qquad (6)$$

It is important to note that not only Ξ needs to be modelled but $|\nabla \bar{c}|$ also needs closure because $\bar{c}$ is also an unknown quantity because a transport equation for $\tilde{c}$ is solved (see eq. 2). This subtlety is ignored in some occasions or alternatively solved using the BML formalism (Bray *et al.*, 1985) in order to express $\bar{c}$ as a function of $\tilde{c}$ using the heat release parameter $\tau = (T_{ad} - T_0)/T_0$ (with T_{ad} and T_0 being the adiabatic flame temperature and unburned gas temperature respectively) in the following manner:

$$\bar{c} = (1 + \tau)\tilde{c} \,/\, (1 + \tau \tilde{c}) \qquad (7)$$

It is reported in the literature that using $|\nabla \bar{c}|$ in conjunction with eq. (7) results in undesirable flame thickening and use of an explicit counter-gradient transport (CGT) model is recommended (Ma *et al.*, 2013). Allauddin *et al.* (2017) argued that replacing $|\nabla \bar{c}|$ with $|\nabla \tilde{c}|$ can be understood as an implicit CGT model. Mathematically, the flame thickening is the result of a steeper (shallower) gradient of $\bar{c}$ obtained near the fresh (burnt) gas side of the flame, as shown in Fig. 1. This acts to increase the value of FSD in the leading edge in comparison to its value towards the burned gas side, which in turn leads to a faster propagation rate at the leading edge than at the trailing edge according to Ma *et al.* (2013).

It is interesting to recall the Favre-filtered *G*-equation (Peters, 2000; Pitsch *et al*., 2002), which describes the location of a thin flame interface and is given by:

$$\bar{\rho}[\partial\tilde{G}/\partial t + \tilde{\boldsymbol{u}} \cdot \nabla\tilde{G}] = \rho_0 \Xi_G S_L |\nabla\tilde{G}| \tag{8}$$

Here, Ξ_G is a wrinkling factor in the context of *G*-equation approach (Peters, 2000). Note, that the same variable, i.e. $\tilde{G}$, is used to express both left and right sides of eq. 8. Upon comparison of eq. 5 in conjunction with eq. 2 with the *G*-equation it becomes clear that the undesirable flame thickening could potentially be avoided by introducing a new definition of the wrinkling factor and resolved FSD as follows:

$$\overline{\nabla \cdot (\rho D \nabla c) + \dot{\omega}_c} = \overline{(\rho S_d)}_S \, \Xi_F \, |\nabla\tilde{c}| \;\; ; \quad \Xi_F = \overline{|\nabla c|}/|\nabla\tilde{c}| \tag{9}$$

The wrinkling factor with a subscript F refers to the alternative definition based on $|\nabla\tilde{c}|$. Formally, the result of combining eq. 2 with eq. 5 is identical to combining eq. 2 with eq. 9. However, existing wrinkling factor models attempt to predict the magnitude of total flame wrinkling by correcting the resolved scalar gradient $|\nabla\bar{c}|$ by the wrinkling factor Ξ. In general, they do not account for the local variation of Ξ with respect to reaction progress variable $\tilde{c}$. In this regard, the alternative definition of flame wrinkling given by eq. 9 might be advantageous. By employing an FFFD model proportional to $|\nabla\tilde{c}|$ some previous analyses (Allauddin *et al*., 2017; Lecocq *et al*., 2010; Ma *et al*. 2013; Keppeler *et al*., 2014) indeed implicitly used the definition given by eq. 9 instead of the conventional definition (i.e. eq. 5) and reported satisfactory agreement with experimental/expected results based on LES. This warrants physical explanations, which are yet to be available in the existing literature. Thus, the goal of this paper is an in-depth comparison of both definitions of wrinkling factor using *a-priori* analysis of planar flame DNS data and to provide physical explanations for the observations made by Allauddin *et al*. (2017), Lecocq *et al*. (2010), Ma *et al*. (2013) and Keppeler *et al*. (2014) based on their respective LES results.

The rest of the paper is organised in the following manner. The details related to the DNS database and its filtering will be explained in the next section. Following this, several existing closures for the FFFD term used in this work will be briefly summarized. This will be followed by the analysis of the models. Finally, conclusions will be drawn.

2. DNS DATABASE

A DNS database of turbulent premixed planar flames with single step Arrhenius type irreversible chemistry has been considered for the current analysis, consisting of two flames (denoted henceforth case A and case B) with global Lewis number Le = 1.0. The turbulent Reynolds number Re_t for cases A and B, normalised turbulent root-mean-square (rms) velocity fluctuation is u'/S_L, integral length scale to thermal flame thickness ratio l/δ_{th}, Damköhler number Da, and Karlovitz number Ka are shown in Table 1. The definitions of these quantities are given as:

$$Da = \frac{lS_L}{\delta_{th}u'} \quad Ka = \left(\frac{u'}{S_L}\right)^{\frac{3}{2}}\left(\frac{l}{\delta_{th}}\right)^{-\frac{1}{2}} \quad \delta_{th} = \frac{T_{ad}-T_0}{\max|\nabla T|_L} \quad \tau = \frac{T_{ad}-T_0}{T_0} \quad \beta = \frac{T_{ac}(T_{ad}-T_0)}{T_{ad}^2} \tag{10}$$

Here S_L is the unstrained laminar burning velocity, δ_{th} is the thermal flame thickness. Note that the subscript 'L' refers to the unstrained laminar flame quantities. The heat release parameter τ and the Zel'dovich number β are taken to be 4.5 and 6.0 respectively where T_{ac} is the activation temperature. Standard values of Prandtl number ($Pr = 0.7$) and ratio of specific heats ($\gamma_g = 1.4$) have been used.

The turbulent velocity fluctuations are initialised using a homogeneous isotropic incompressible velocity field in conjunction with a model spectrum suggested in Pope (2000). The reacting flow field is initialised by a steady planar unstrained premixed laminar flame solution. In all cases flame-turbulence interaction takes place under decaying turbulence and

all the non-dimensional numbers mentioned before have to be understood as initial values here and in the remainder of the text. The simulation time is chosen to be larger than the chemical time scale as well as the eddy turnover time when turbulent flame area and the kinetic energy of fluid evaluated over the whole volume were no longer varying rapidly with time. The simulation domain is taken to be a cube of $26.1\ \delta_{th} \times 26.1\ \delta_{th} \times 26.1\ \delta_{th}$ which is discretised using a uniform Cartesian grid of 512×512×512 points ensuring 11 grid points are kept within δ_{th}. Spatial derivatives for all internal grid points are evaluated using a 10th order central difference scheme but the order of discretization gradually drops to a one-sided 2nd order scheme at the non-periodic boundaries. Time integration is carried out using an explicit 3rd order low storage Runge-Kutta scheme. The boundary conditions in the mean flame propagation direction (aligned with negative x_1-direction) are taken to be partially non-reflecting, whereas boundaries in transverse directions are taken to be periodic. Similar DNS databases have been considered previously by the authors (for more details see Chakraborty *et al.*, 2011; Chakraborty *et al*., 2009), but the present database extends the earlier ones to higher turbulent Reynolds number and a larger scale separation l/δ_{th}.

For the purpose of the *a-priori* analysis carried out in this work, the DNS data has been explicitly filtered using a Gaussian filter kernel (see Eq.1). Results will be presented from $\Delta \approx 0.4\ \delta_{th}$ where the flame is almost resolved, up to $\Delta \approx 5.6\ \delta_{th}$ where the flame becomes fully unresolved and Δ is at the order of the integral length scale l. The result of the explicit filtering operation is a 512^3 dataset, with the same dimensions as the original DNS database. If during *a-priori* analysis, a model expression is evaluated based on the filtered data one has to decide if gradients of the variable under consideration are evaluated numerically based on the DNS grid (filter) size Δ_{DNS} or based on the size of the convolution filter Δ_{conv} which corresponds in our case: $\Delta_{conv} = n\Delta_{DNS}$ with $n = 4,16,28,56$. Throughout this work the expressions $|\nabla \tilde{c}|$

and $|\nabla \tilde{c}|$ will be evaluated using Δ_{conv} based on finite difference formulae. As a result, these terms will contain realistic truncation errors.

3. ALGEBRAIC WRINKLING FACTOR MODELS

A large variety of wrinkling factor based algebraic FSD models has been analysed in detail in Chakraborty and Klein, (2008) and Ma *et al.* (2013). The present analysis focuses on a small selection of wrinkling factor models (Angelberger *et al*. 1998; Charlette *et al*. 2002; Fureby 2005; Gülder 1990; Pocheau 1994; Zimont 1995) which can be written in the form of eq. 5 i.e. the resolved FSD can be factored in: $\Sigma_{\mathrm{gen}} = \Xi \cdot |\nabla \bar{c}|$. These wrinkling factor expressions expressions are given in alphabetical order in Table 2. For a discussion of these models we refer the reader to the original references or the summary provided in Chakraborty and Klein, (2008) and Ma *et al.* (2013).

4. RESULTS & DISCUSSION

In an earlier analysis by these authors (Chakraborty and Klein, 2008) the performance of different algebraic LES FSD models has been assessed with respect to three criteria:

(i) The volume-averaged value of the generalised FSD $< \Sigma_{gen} >$ represents the total flame surface area. Thus it should not vary with Δ and should be equal to the corresponding value obtained from the DNS data.

(ii) The correlation coefficient between the modelled FSD and the FSD obtained from DNS database should be as close to unity as possible.

(iii) The model should be able to capture the correct variation of conditionally averaged values of Σ_{gen} with filtered reaction progress variable $\bar{c}$ across the flame brush.

The same methodology will be used in this work with the exception that Σ_{gen} will be expressed either as $\Sigma_{gen} = \Xi_{model}|\nabla \bar{c}|$ or $\Sigma_{gen} = \Xi_{model}|\nabla \tilde{c}|$ where Ξ_{model} is one of the existing models

for Ξ given in Table 2. In addition, the behaviour of Ξ extracted from explicitly filtered DNS data will be compared to that of Ξ_F.

The goal of this work is to show that existing wrinkling factor models can also be used to model Ξ_F rather than comparing individual models with each other, which has already been discussed extensively in Chakraborty and Klein (2008) and Ma *et al.* (2013).

Figure 3 shows the variation of volume-averaged Σ_{gen} with Δ/δ_{th} for cases A and B. The modelling according to eq. 5 is shown on the left, whereas the results according to alternative definition are shown in the right column. The volume-averaged flame surface area is a quantity of primary interest and Fig. 3 clearly shows that existing wrinkling factor models work equally well for modelling both $< \Xi|\nabla\bar{c}| >$ and $< \Xi_F|\nabla\tilde{c}| >$.

In contrast to the volume-averaged FSD, the volume-averaged wrinkling factor is expected to increase with increasing filter size, because it represents the ratio of total to resolved flame wrinkling and the latter quantity decreases with increasing filter size. The variations of volume-averaged modelled wrinkling factors $< \Xi >$ and $< \Xi_F >$ with normalized filter width are shown in Fig. 4 for both cases. It can be seen from Fig. 4 that $< \Xi_F >$ gives slightly higher values compared to $< \Xi >$. Furthermore the prediction of the Fureby model is close to the actual DNS value of $< \Xi >$, whereas the other models tend to overpredict the flame wrinkling with increasing filter size. It is also worth noting that all models approach the correct asymptotic limit of unity (i.e. $lim_{\Delta\to 0}\Sigma_{gen} = lim_{\Delta\to 0}|\nabla\bar{c}| = lim_{\Delta\to 0}|\nabla\tilde{c}| = |\nabla c|$ and thus $\Xi = \Xi_F = 1.0$) in the limit of small filter size.

A comparison between Fig. 3 and Fig. 4 reveals that the value of $< \Sigma_{gen} >$ is more or less equally over- and underpredicted by the different models (see Fig. 3), whereas $< \Xi >$ is overpredicted by all models except for the Fureby model.

The explanation for this behaviour can be obtained from Fig. 5 where the variation of volume-averaged resolved FSD with normalised filter size Δ/δ_{th} is shown for cases A and B according to the conventional definition based on $|\nabla\bar{c}|$ as well as for the alternative definition in terms of $|\nabla\tilde{c}|$. For small filter size, the magnitude of the volume-averaged resolved FSD is close to the value of volume-averaged generalised FSD (because $lim_{\Delta\to 0}\Sigma_{gen} = lim_{\Delta\to 0}|\nabla\bar{c}| = lim_{\Delta\to 0}|\nabla\tilde{c}| = |\nabla c|$), as shown in Fig. 3. For increasing filter size the value of volume-averaged resolved FSD decreases due to two effects which can be distinguished by approximating $\nabla\bar{c}$ and $\nabla\tilde{c}$ using DNS grid or LES grid based finite differences. In the case of DNS grid based finite differences the decreasing trend can be attributed to the effect of filtering reaction progress variable with increasing filter sizes. The same effect is there for LES grid based finite differences but in addition to this, the effects of truncation errors are now clearly visible. For this reason, the Fureby model predicts the wrinkling factor very well (see Fig. 4) but to some extent underpredicts the volume averaged generalized FSD (see Fig. 3) for this database. This indicates that in general the best model might not be the one that gives the best representation of the wrinkling factor. Instead a model that moderately overpredicts the flame wrinkling and therefore to some extent implicitly accounts for (i.e. counters the effects of) truncation errors might be more successful in an overall basis. This highlights also the close interaction of modelling and numerical errors in LES.

The next focus is on criterion (ii) i.e. the correlation between model expressions and the corresponding values determined from *a-priori* filtered DNS data. For all cases the correlations

between modelled and actual wrinkling are negligibly small, of the order of 0.1 and hence are not shown here. The reason is, that the wrinkling factor models considered here do not contain a dependence on $\tilde{c}$ or its gradient, but instead depend on the state of local turbulence. Because of the poor correlation between Ξ or Ξ_F with Ξ_{model}, it can be inferred that the correlation between Σ_{gen} and $\Xi_{\mathrm{model}}|\nabla\bar{c}|$ and between $\Xi_{\mathrm{model}}|\nabla\tilde{c}|$ depends primarily on the correlation between $\overline{|\nabla c|}$ and $|\nabla\bar{c}|$ or $|\nabla\tilde{c}|$. As a consequence, the correlation coefficients for the different models show a relatively small variation (maximum 0.05 around the mean) and only the average correlation coefficients over all models for a particular filter size are shown in Fig. 6. It can be seen from Fig. 6 that the correlation strength decreases considerably with increasing filter size. The correlation strength is slightly lower for Case B with the higher turbulence intensity and correlations involving $\tilde{c}$ are slightly higher compared to those using $\bar{c}$. The fact that correlations involving $\bar{c}$ do not differ much from correlations involving $\tilde{c}$ has been discussed in Klein *et al.* (2016b) for a different database. It has been argued by Klein *et al.* (2016b) that the spectral content of $\tilde{c}$ and $\bar{c}$ differs mainly at high wavenumbers, i.e. the part which is in the sub-filter range. If $\tilde{c}$ and $\bar{c}$ are sampled and differentiated on a coarse grid, the Nyquist theorem shows that only the lowest frequencies play key roles, and this is exactly the frequency range where both quantities are similar in terms of their frequency content. Overall, the differences between both approaches can be considered to be small in terms of their correlation strengths.

Next, the variation of conditionally averaged values of Σ_{gen} with filtered reaction progress variable $\bar{c}$ across the flame brush will be discussed (criterion (iii)). Results are shown in Fig. 7 for case A and four different filter width. Case B behaves qualitatively very similarly and thus is not shown here. The different magnitudes of the model expressions were evident in the volume-averaged values of generalised FSD in Fig. 3. For small filter size the differences

between $\Xi|\nabla\bar{c}|$ and $\Xi|\nabla\tilde{c}|$ are small because $lim_{\Delta\to 0}|\nabla\bar{c}| = lim_{\Delta\to 0}|\nabla\tilde{c}| = |\nabla c|$ and thus $\Xi = \Xi_F = 1.0$. However, for larger filter size $\Xi|\nabla\bar{c}|$ becomes skewed towards the fresh gas side whereas $\Xi|\nabla\tilde{c}|$ becomes skewed toward the burned gas side. In both cases the conditionally averaged profiles are considerably wider than the generalised FSD. Again it is noted that expressions $|\nabla\bar{c}|$ and $|\nabla\tilde{c}|$ are evaluated using finite differences on the LES grid spacing Δ_{conv}, in contrast to previous analyses (e.g. Chakraborty and Klein (2008)) where the gradients have been calculated on the DNS grid.

Finally, the variation of conditionally averaged wrinkling factors is shown for both cases and two filter widths in Fig. 8. For small filter width (top of figure) the variation of Ξ across the flame brush is relatively small. In particular, both Charlette and Fureby models yield nearly constant values close to unity. However, the variation of Ξ increases considerably with increasing filter width and increasing turbulence intensity. It is also worth noting that Ξ exhibits a smaller degree of variation than the alternative definition Ξ_F. Furthermore, Ξ_F can assume a value smaller than unity but the minimum possible value of Ξ remains unity. Both of these aspects could be considered a disadvantage of the alternative definition Ξ_F. However, since the wrinkling factor models according to conventional definition do not follow the same behaviour as obtained from DNS data, this theoretical disadvantage might be of a minor practical importance.

5. CONCLUSIONS

Algebraic FSD models in conjunction with a wrinkling factor expression, which multiplies the resolved scalar gradient magnitude are one of the standard approaches for modelling turbulent premixed combustion. A drawback in this well-known framework is that the resolved FSD $|\nabla\bar{c}|$ is an unknown quantity because transport equations are typically solved in the context of Favre

filtering. Using BML theory $\bar{c}$ can be expressed using the Favre filtered reaction progress variable $\tilde{c}$. However, this gives rise to additional modelling errors because the assumptions of the BML formalism might not always be fulfilled. Furthermore, it is reported in the literature (Ma *et al.*, 2013) that the use of $|\nabla\bar{c}|$ can result in artificial flame thickening as a result of a steeper (shallower) gradient of $\bar{c}$ obtained near the fresh (burnt) gas side of the flame compared to $\tilde{c}$. This artificial flame thickening can be prevented either by using an explicit counter-gradient transport model or alternatively by numerical methods. In this work an alternative definition of the resolved FSD in terms of Favre filtered reaction progress variable is suggested $|\nabla\tilde{c}|$ which gives rise to an alternative definition of the wrinkling factor $\Xi_F = \overline{|\nabla c|}/|\nabla\tilde{c}|$. In order to compare both definitions a new database of statistically planar turbulent premixed flames with larger scale separation and higher turbulent Reynolds numbers compared to earlier work by the authors (Gao *et al.*, 2015; Chakraborty and Klein, 2008; Ma *et al.*, 2013) has been considered. This database has been explicitly filtered and model expressions have been assessed in the context of *a-priori* analysis. Six different well-known models have been taken from literature and it has been shown that the existing wrinkling factor expressions serve equally well the purpose of modelling either Ξ or Ξ_F. Correlation strengths of modelled generalised FSD with the corresponding variable extracted from DNS are found to be comparable. A minor theoretical disadvantage of the new approach is that Ξ_F shows a somewhat larger variation across the flame brush compared to Ξ. However, the advantages of the new formulation are that it results in a closed form expression of the resolved FSD and that artificial flame thickening can be avoided without resorting to an explicit counter-gradient transport modelling. Furthermore, the close interaction between physical modelling and numerical errors in a LES has been highlighted by evaluating and comparing the volume averaged resolved FSD (a quantity proportional to resolved flame area) on the DNS grid and the corresponding LES grid size. The results on the DNS grid reflect only the effect of filtering

and modelling inaccuracies, whereas numerical errors and its interaction with modelling errors become important when finite differences with the equivalent LES grid are used for evaluating the resolved FSD. It is worth noting that the alternative definition of the wrinkling factor and the present *a-priori* DNS analysis provide a physical and theoretical justifications for the observation (Allauddin *et al*., 2017; Ma *et al*., 2013; Lecocq *et al*., 2010; Keppeler *et al*., 2014) that satisfactory LES results can be obtained by replacing $|\nabla \bar{c}|$ with $|\nabla \tilde{c}|$.

ACKNOWLEDGEMENTS

The authors are grateful to N8, ARCHER and EPSRC for computational support.

REFERENCES

Allaudin U., Klein M., Pfitzner M. and Chakraborty N. 2017. A-priori and a-posteriori analysis of algebraic flame surface density modeling in the context of Large Eddy Simulation of turbulent premixed combustion. Numer. Heat Trans. A, 71,153-171.

Angelberger, C., Veynante, D., Egolfopoulos, F., and Poinsot, T. 1998. A flame surface density model for Large Eddy Simulations of turbulent premixed flames, Proc.of the Summer Program, Center for Turbulence Research, Stanford 66-82.

Boger, M., Veynante, D., Boughanem, H. and Trouvé, A. 1998. Direct Numerical Simulation analysis of flame surface density concept for Large Eddy Simulation of turbulent premixed combustion, Proc. Combust. Inst., 27: 917-925.

Bray, K.N.C., Libby, P.A., Moss, J. B. 1985. Unified modelling approach for premixed turbulent combustion – Part I: General Formulation, Combust. Flame, 61:87-102.

Chakraborty, N. and Klein M. 2008. A-priori direct numerical simulation assessment of algebraic flame surface density models for turbulent premixed flames in the context of large eddy simulation, Phys. Fluids, 20:085108.

Chakraborty, N. , Klein, M., Swaminathan, N. 2009. Effects of Lewis number on the reactive scalar gradient alignment with local strain rate in turbulent premixed flames. Proceedings of the Combustion Institute, 32, 1409-1417.

Chakraborty, N., Klein M. and Cant R.S. 2011. Effects of turbulent Reynolds number on the displacement speed statistics in the thin reaction zones regime of turbulent premixed combustion, Journal of Combustion, Article number 473679.

Charlette, F., Meneveau, C. and Veynante, D. 2002. A power-law flame wrinkling model for LES of premixed turbulent combustion. Part I: Non-dynamic formulation and initial tests, Combust. Flame, 131 159-180.

Colin, O., Ducros, F., Veynante, D. and Poinsot, T. 2000. A thickened flame model for large eddy simulations of turbulent premixed combustion, Phys. Fluids, 12(7): 1843-1863.

Fureby, C. 2005. A fractal flame wrinkling large eddy simulation model for premixed turbulent combustion, Proc. Combust. Inst. 30 593-601.

Gao, Y., Chakraborty, N. and Klein, M. 2015. Assessment of the performances of sub-grid scalar flux models for premixed flames with different global Lewis numbers: a Direct Numerical Simulation analysis. Int. J. Heat Fluid Flow, 52, 28–39.

Gülder, O. 1990. Turbulent premixed combustion modelling using fractal geometry, Proc. Combust. Inst. 23 835-841.

Keppeler R., Tangermann E., Allaudin U., and Pfitzner M. 2014. LES of Low to High Turbulent Combustion in an Elevated Pressure Environment, Flow Turb. Combust., 92, 767-802.

Klein, M., Chakraborty, N. Gao, Y. 2016a. Scale similarity based models and their application to subgrid scale scalar flux modelling in the context of turbulent premixed flames. International Journal of Heat and Fluid Flow, 57, 91–108.

Klein, N., Chakraborty, N. and Pfitzner, M. 2016b. Analysis of the combined modeling of subgrid transport and filtered flame propagation for premixed turbulent combustion. Flow Turb. Combust., 96, 921-938.

Lecocq, G., Richard, S., Colin, O., Vervisch, L. 2010. Gradient and counter-gradient modelling in premixed flames: theoretical study and application to the LES of a Lean premixed turbulent swirl-burner, Combust. Sci. Technol., Vol.182, pp. 465-479.

Ma., T., Stein, T.O., Chakraborty, N. and Kempf A.M. 2013. A posteriori testing of algebraic flame surface density models for LES, Combust. Theor. and Modell., , 17:431-482.

Pitsch, H., and Duchamp de Lageneste, H. 2002. Large-eddy simulation of premixed turbulent combustion using a level-set approach, Proc. Combust. Inst. 29: 2001-2008.

Peters, N. 2000. Turbulent Combustion, Cambridge University Press, UK.

Pocheau, A. 1994. Scale invariance in turbulent front propagation, Phys. Rev. E 49 1109-1122.

Pope, B.P. 2000. Turbulent flows, Cambridge University Press.

Zimont, V. L., Lipatnikov A. 1995. A numerical model of premixed turbulent combustion of gases, Chem. Phys. Rep. 4 993-1025.

TABLES

Case	Re_t	u'/S_L	l/δ_{th}	Da	Ka
A	87.5	7.5	4.58	0.61	9.6
B	175.0	15.0	4.58	0.31	27.16

Table 1: Characteristic parameters for the two planar turbulent premixed flames considered in this analysis.

ANGELBERGER	$\Xi = [1 + a\Gamma.(u'_\Delta / S_L)]$ $u'_\Delta = \sqrt{2k/3}$, $\Gamma = 0.75\exp\left[-1.2/(u'_\Delta / S_L)^{0.3}\right](\Delta/\delta_L)^{2/3}$
CHARLETTE	$\Xi = \left(1 + \min\left[\Delta/\delta_L, \Gamma_\Delta.(u'/S_L)\right]\right)^{\beta_1}$, b_1=1.4, β_1=0.5, $\mathrm{Re}_\Delta = u'_\Delta.\Delta/\nu$ $\Gamma_\Delta = [((f_u^{-a_1} + f_\Delta^{-a_1})^{-1/a_1})^{-b_1} + f_{\mathrm{Re}}^{-b_1}]^{-1/b_1}$, $f_u = 4\left(\frac{27C_k}{110}\right)^{1/2}\left(\frac{18C_k}{55}\right)\left(\frac{u'_\Delta}{S_L}\right)^2, C_k = 1.5$ $f_\Delta = \left[\frac{27C_k\pi^{4/3}}{110}\times\left(\left(\frac{\Delta}{\delta_L}\right)^{4/3} - 1\right)\right]^{1/2}$, $f_{\mathrm{Re}} = \left[\frac{9}{55}\exp\left(-\frac{3}{2}C_k\pi^{4/3}\,\mathrm{Re}_\Delta^{-1}\right)\right]^{1/2}\times\mathrm{Re}_\Delta^{1/2}$ $a_1 = 0.60 + 0.20\exp[-0.1(u'/S_L)] - 0.20\exp[-0.01(\Delta/\delta_L)]$.
FUREBY **(MODIFED)**	$\Xi = [1 + \Gamma.(u'_\Delta / S_L)]^{D-2}$, where Γ is the same as in the ANGELBERGER model and D is given by $= 2.05/(u'_\Delta/S_L + 1) + 2.35/(S_L/u'_\Delta + 1)$.
GÜLDER	$\Xi = [1 + 0.62\sqrt{u'_\Delta / S_L}.(u'_\Delta\eta/\nu)]$
POCHEAU	$\Xi = [1 + c_1(u'_\Delta / S_L)^{c_2}]^{1/c_2}$, c_1 =1.0, c_2 =2.0;
ZIMONT	$\Xi = [1 + 0.51.(u'_\Delta / S_L)^{3/4}(\Delta/\delta_L)^{1/4}]$

Table 2: List of algebraic wrinkling factor models considered here where ν is the kinematic viscosity in the unburned gas and $\delta_L = \alpha_{T0}/S_L$ is the Zel'dovich flame thickness with α_{T0} being thermal diffusivity in the unburned gas.

FIGURE CAPTIONS

Figure 1. Sketch of a 1D laminar back to back flame. Profiles of (a) normalised density ρ/ρ_0 and reaction progress variable c as well as filtered $\bar{c}$ and Favre filtered $\tilde{c}$ reaction progress variable, assuming a filter size of $\Delta/\delta_{th} = 2.8$; (b) Magnitudes of $\partial\bar{c}/\partial x$ and $\partial\tilde{c}/\partial x$ normalized with δ_{th}.

Figure 2. Instantaneous view of c isosurfaces for cases A and B. The value of c increases from 0.1 (yellow) to 0.9 (red).

Figure 3. Variation of volume-averaged generalised FSD $< \Sigma_{gen} >$ with normalised filter size Δ/δ_{th} for case A (top) and case B (bottom). The standard modelling approach according to eq. 5 is shown in the left column, the new approach (see eq. 9) is shown in the right column.

Figure 4. Variation of volume-averaged wrinkling factor with normalised filter size Δ/δ_{th} for case A (left) and case B (right).

Figure 5. Variation of volume-averaged resolved FSD with normalised filter size Δ/δ_{th} according to the conventional definition (i.e. $|\nabla\bar{c}|$) as well as according to the alternative definition (i.e. $|\nabla\tilde{c}|$) for cases A and B. Finite differences are either evaluated on the DNS grid or the LES grid for comparison.

Figure 6. Correlation coefficients between Σ_{gen} and $\Xi_{\mathrm{model}}|\nabla\bar{c}|$ (left figure) respectively $\Xi_{\mathrm{model}}|\nabla\tilde{c}|$ (right figure) for cases A and B and four different filter width.

Figure 7. Variation of conditionally averaged generalised FSD for case A and four different filter sizes (from top to bottom $\Delta/\delta_{th} = 0.4, 1.6, 2.8, 5.6$). The standard modelling approach according to eq. 5 is shown in the left column the new approach (see eq. 9) is shown on the right.

Figure 8. Variation of conditionally averaged wrinkling factor for case A and B exemplarily shown for two filter sizes ($\Delta/\delta_{th} = 0.4, 5.6$).

FIGURES

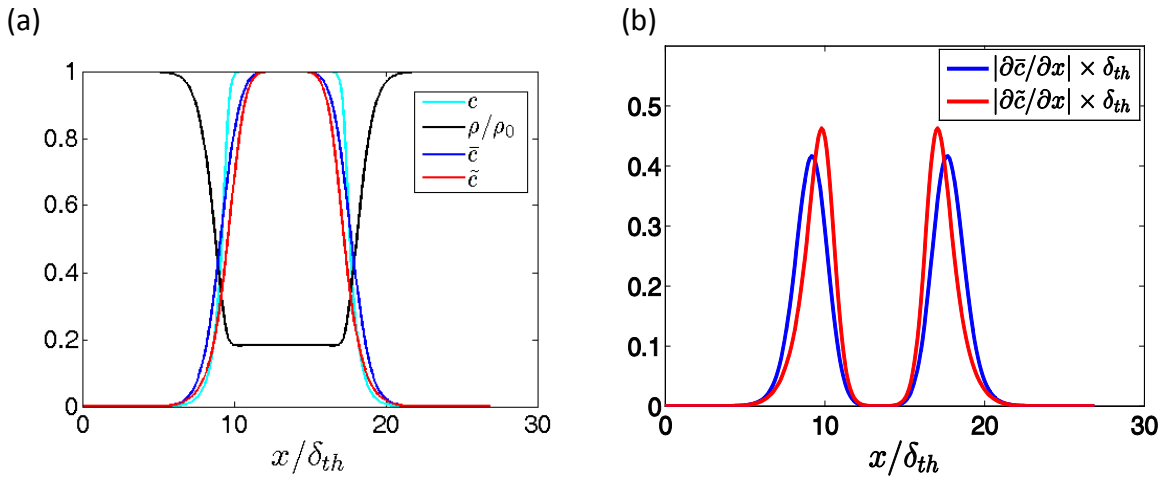

Figure 1. Sketch of a 1D laminar back to back flame. Profiles of (a) normalised density ρ/ρ_0 and reaction progress variable c as well as filtered $\bar{c}$ and Favre filtered $\tilde{c}$ reaction progress variable, assuming a filter size of $\Delta/\delta_{th} = 2.8$; (b) Magnitudes of $\partial\bar{c}/\partial x$ and $\partial\tilde{c}/\partial x$ normalized with δ_{th}.

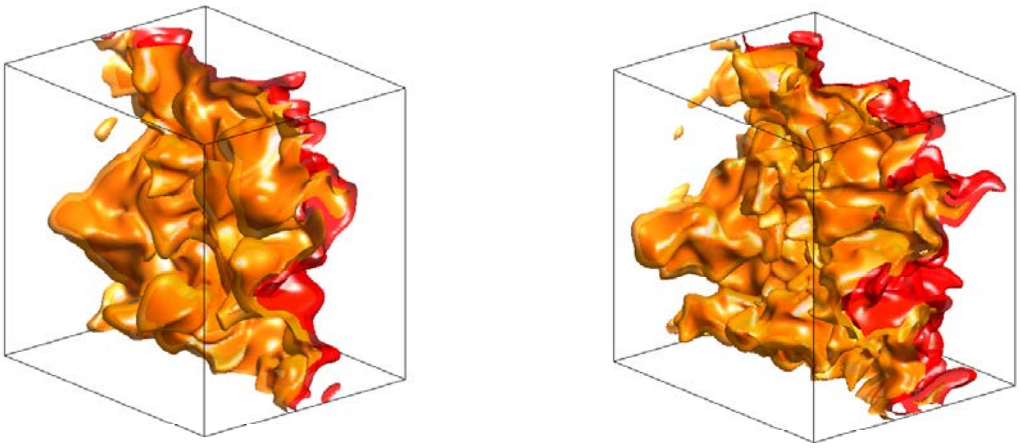

Figure 2. Instantaneous view of *c* isosurfaces for cases A and B. The value of *c* increases from 0.1 (yellow) to 0.9 (red).

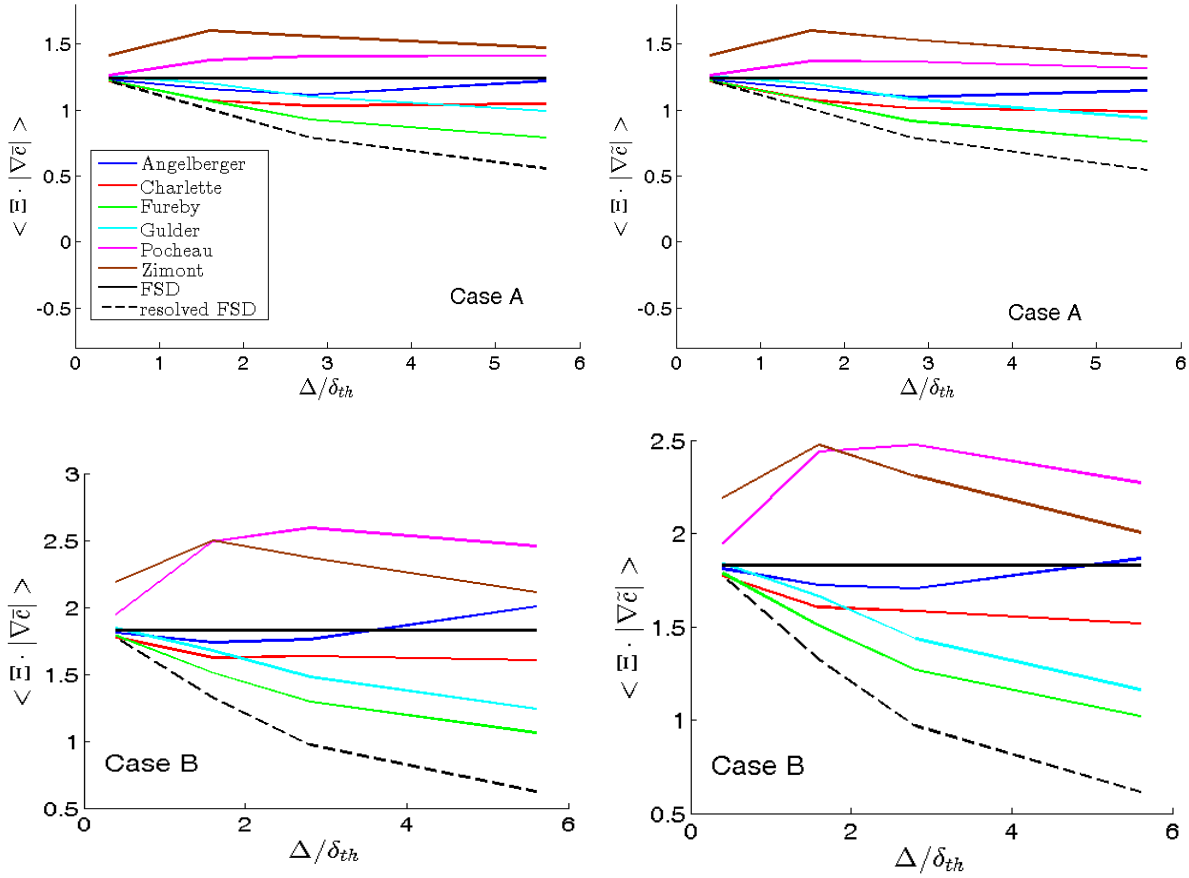

Figure 3. Variation of volume-averaged generalised FSD $< \Sigma_{gen} >$ with normalised filter size Δ/δ_{th} for case A (top) and case B (bottom). The standard modelling approach according to eq. 5 is shown in the left column, the new approach (see eq. 9) is shown in the right column.

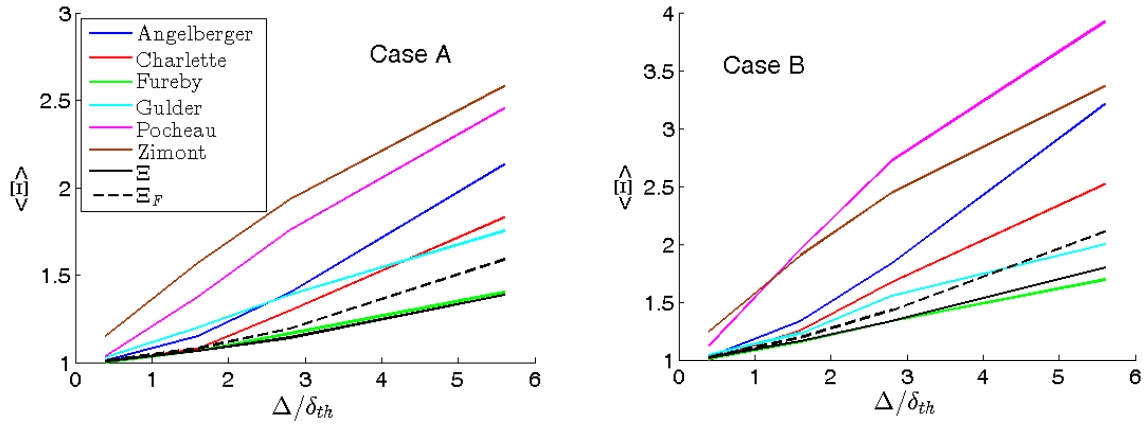

Figure 4. Variation of volume-averaged wrinkling factor with normalised filter size Δ/δ_{th} for case A (left) and case B (right).

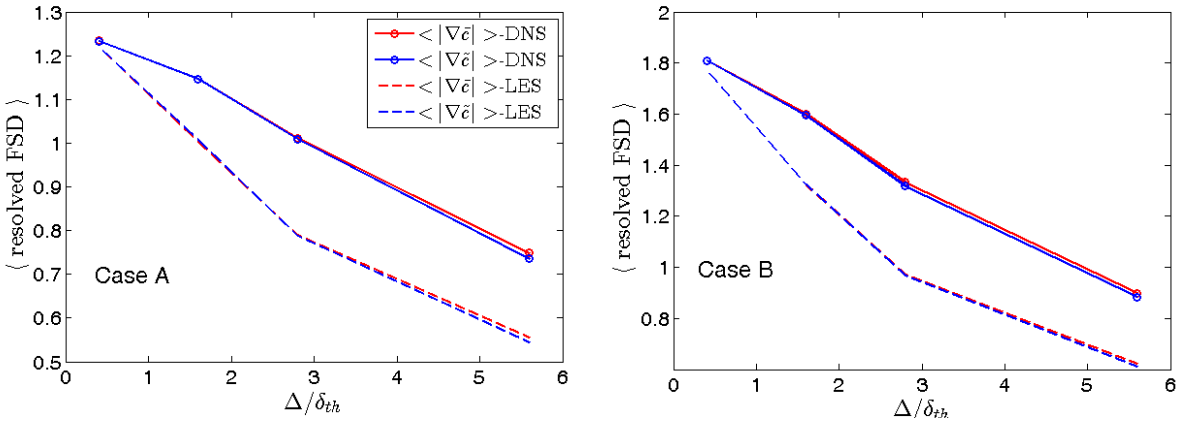

Figure 5. Variation of volume-averaged resolved FSD with normalised filter size Δ/δ_{th} according to the conventional definition (i.e. $|\nabla\bar{c}|$) as well as according to the alternative definition (i.e. $|\nabla\tilde{c}|$) for cases A and B. Finite differences are either evaluated on the DNS grid or the LES grid for comparison.

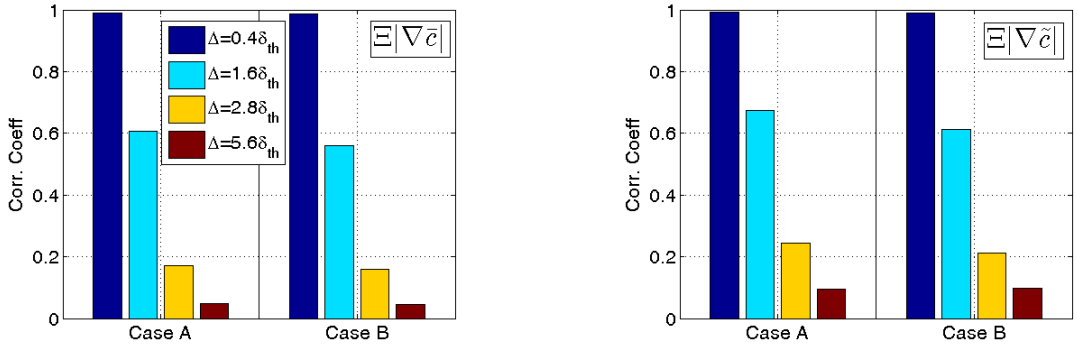

Figure 6. Correlation coefficients between Σ_{gen} and $\Xi_{\mathrm{model}}|\nabla\bar{c}|$ (left figure) respectively $\Xi_{\mathrm{model}}|\nabla\tilde{c}|$ (right figure) for cases A and B and four different filter width.

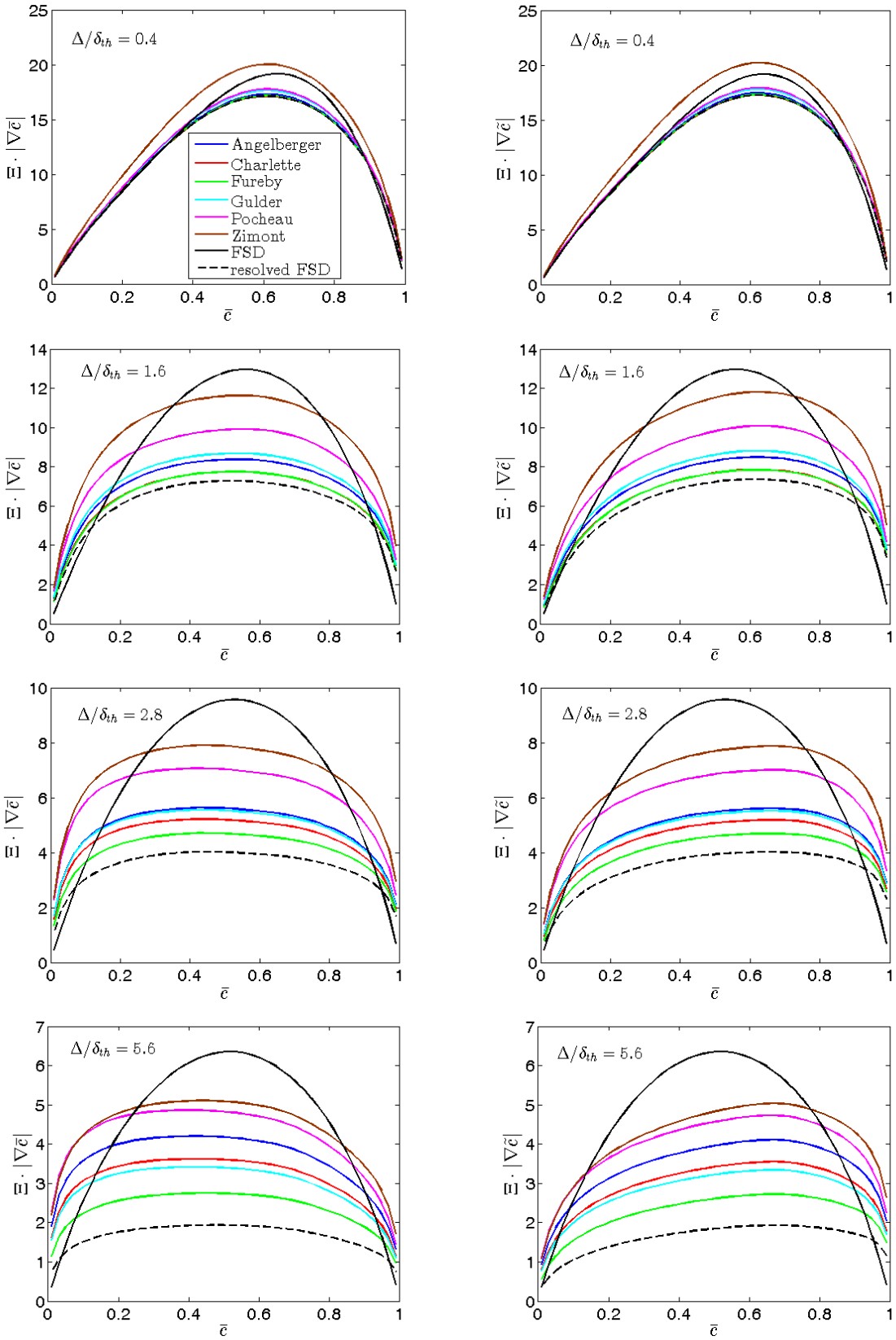

Figure 7. Variation of conditionally averaged generalised FSD for case A and four different filter sizes (from top to bottom $\Delta/\delta_{th} = 0.4, 1.6, 2.8, 5.6$). The standard modelling approach according to eq. 5 is shown in the left column the new approach (see eq. 9) is shown on the right.

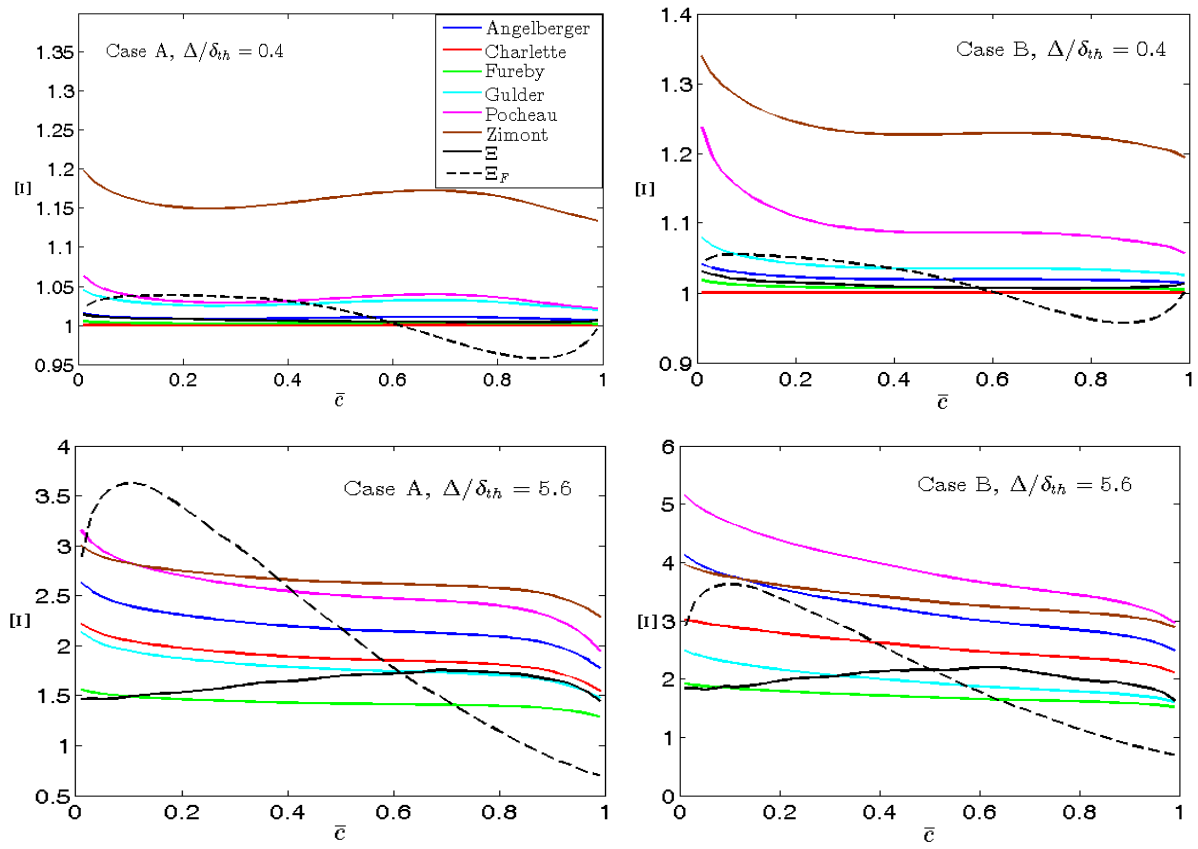

Figure 8. Variation of conditionally averaged wrinkling factor for case A and B exemplarily shown for two filter sizes ($\Delta/\delta_{th} = 0.4, 5.6$).